

We perform a time-dependent Dalitz plot analysis of $B^0 \rightarrow K_S^0 \pi^+ \pi^-$ in order to extract the CP violation parameters of $f_0(980)K_S^0$ and $\rho^0(770)K_S^0$ and direct CP -asymmetries of $K^{*+}(892)\pi^-$. The results are obtained from a data sample of $(383 \pm 3) \times 10^6$ $B\bar{B}$ decays, collected with the BaBar detector at the PEP2 asymmetric-energy B factory at SLAC. The measured values of $2\beta_{\text{eff}}$ in B^0 decays to $f_0(980)K_S^0$ and $\rho^0(770)K_S^0$ are $(89_{-20}^{+22} \pm 5 \pm 8)^\circ$ and $(37_{-17}^{+19} \pm 5 \pm 6)^\circ$, respectively, where the first quoted uncertainty is statistical, the second is systematic and the third is Dalitz plot signal model uncertainty. We measure the significance of $2\beta_{\text{eff}}(f_0(980)K_S^0) \neq 0$ to be 4.3σ . In decays to $K^*(892)\pi$ we find $A_{CP} = -0.18 \pm 0.10 \pm 0.03 \pm 0.03$. The measured phase difference between the decay amplitudes of $B^0 \rightarrow K^{*+}(892)\pi^-$ and $\bar{B}^0 \rightarrow K^{*-}(892)\pi^+$ is $(-164 \pm 24 \pm 12 \pm 15)^\circ$. All results are preliminary.

Time-dependent Dalitz Plot Analysis of $B^0 \rightarrow K_S^0 \pi^+ \pi^-$

The BABAR Collaboration

November 1, 2018

Abstract

We perform a time-dependent Dalitz plot analysis of $B^0 \rightarrow K_S^0 \pi^+ \pi^-$ in order to extract the CP violation parameters of $f_0(980)K_S^0$ and $\rho^0(770)K_S^0$ and direct CP -asymmetries of $K^{*+}(892)\pi^-$. The results are obtained from a data sample of $(383 \pm 3) \times 10^6$ $B\bar{B}$ decays, collected with the BABAR detector at the PEP-II asymmetric-energy B factory at SLAC. The measured values of $2\beta_{\text{eff}}$ in B^0 decays to $f_0(980)K_S^0$ and $\rho^0(770)K_S^0$ are $(89_{-20}^{+22} \pm 5 \pm 8)^\circ$ and $(37_{-17}^{+19} \pm 5 \pm 6)^\circ$, respectively, where the first quoted uncertainty is statistical, the second is systematic and the third is Dalitz plot signal model uncertainty. We measure the significance of $2\beta_{\text{eff}}(f_0(980)K_S^0) \neq 0$ to be 4.3σ . In decays to $K^*(892)\pi$ we find $A_{CP} = -0.18 \pm 0.10 \pm 0.03 \pm 0.03$. The measured phase difference between the decay amplitudes of $B^0 \rightarrow K^{*+}(892)\pi^-$ and $\bar{B}^0 \rightarrow K^{*-}(892)\pi^+$ is $(-164 \pm 24 \pm 12 \pm 15)^\circ$. All results are preliminary.

Contributed to the XXIIIrd International Symposium on Lepton and Photon Interactions at High Energies, 8/13 – 8/18/2007, Daegu, Korea

Stanford Linear Accelerator Center, Stanford University, Stanford, CA 94309

Work supported in part by Department of Energy contract DE-AC03-76SF00515.

The BABAR Collaboration,

B. Aubert, M. Bona, D. Boutigny, Y. Karyotakis, J. P. Lees, V. Poireau, X. Prudent, V. Tisserand,
A. Zghiche

*Laboratoire de Physique des Particules, IN2P3/CNRS et Université de Savoie, F-74941 Annecy-Le-Vieux,
France*

J. Garra Tico, E. Grauges

Universitat de Barcelona, Facultat de Física, Departament ECM, E-08028 Barcelona, Spain

L. Lopez, A. Palano, M. Pappagallo

Università di Bari, Dipartimento di Fisica and INFN, I-70126 Bari, Italy

G. Eigen, B. Stugu, L. Sun

University of Bergen, Institute of Physics, N-5007 Bergen, Norway

G. S. Abrams, M. Battaglia, D. N. Brown, J. Button-Shafer, R. N. Cahn, Y. Groyzman, R. G. Jacobsen,
J. A. Kadyk, L. T. Kerth, Yu. G. Kolomensky, G. Kukartsev, D. Lopes Pegna, G. Lynch, L. M. Mir,
T. J. Orimoto, I. L. Osipenkov, M. T. Ronan,¹ K. Tackmann, T. Tanabe, W. A. Wenzel

Lawrence Berkeley National Laboratory and University of California, Berkeley, California 94720, USA

P. del Amo Sanchez, C. M. Hawkes, N. Soni, A. T. Watson

University of Birmingham, Birmingham, B15 2TT, United Kingdom

H. Koch, T. Schroeder

Ruhr Universität Bochum, Institut für Experimentalphysik 1, D-44780 Bochum, Germany

D. Walker

University of Bristol, Bristol BS8 1TL, United Kingdom

D. J. Asgeirsson, T. Cuhadar-Donszelmann, B. G. Fulsom, C. Hearty, T. S. Mattison, J. A. McKenna

University of British Columbia, Vancouver, British Columbia, Canada V6T 1Z1

M. Barrett, A. Khan, M. Saleem, L. Teodorescu

Brunel University, Uxbridge, Middlesex UB8 3PH, United Kingdom

V. E. Blinov, A. D. Bukin, V. P. Druzhinin, V. B. Golubev, A. P. Onuchin, S. I. Serednyakov,
Yu. I. Skovpen, E. P. Solodov, K. Yu. Todyshev

Budker Institute of Nuclear Physics, Novosibirsk 630090, Russia

M. Bondioli, S. Curry, I. Eschrich, D. Kirkby, A. J. Lankford, P. Lund, M. Mandelkern, E. C. Martin,
D. P. Stoker

University of California at Irvine, Irvine, California 92697, USA

S. Abachi, C. Buchanan

University of California at Los Angeles, Los Angeles, California 90024, USA

S. D. Foulkes, J. W. Gary, F. Liu, O. Long, B. C. Shen,¹ G. M. Vitug, L. Zhang

University of California at Riverside, Riverside, California 92521, USA

¹Deceased

H. P. Paar, S. Rahatlou, V. Sharma

University of California at San Diego, La Jolla, California 92093, USA

J. W. Berryhill, C. Campagnari, A. Cunha, B. Dahmes, T. M. Hong, D. Kovalskyi, J. D. Richman

University of California at Santa Barbara, Santa Barbara, California 93106, USA

T. W. Beck, A. M. Eisner, C. J. Flacco, C. A. Heusch, J. Kroseberg, W. S. Lockman, T. Schalk,
B. A. Schumm, A. Seiden, M. G. Wilson, L. O. Winstrom

University of California at Santa Cruz, Institute for Particle Physics, Santa Cruz, California 95064, USA

E. Chen, C. H. Cheng, F. Fang, D. G. Hitlin, I. Narsky, T. Piatenko, F. C. Porter

California Institute of Technology, Pasadena, California 91125, USA

R. Andreassen, G. Mancinelli, B. T. Meadows, K. Mishra, M. D. Sokoloff

University of Cincinnati, Cincinnati, Ohio 45221, USA

F. Blanc, P. C. Bloom, S. Chen, W. T. Ford, J. F. Hirschauer, A. Kreisel, M. Nagel, U. Nauenberg,
A. Olivas, J. G. Smith, K. A. Ulmer, S. R. Wagner, J. Zhang

University of Colorado, Boulder, Colorado 80309, USA

A. M. Gabareen, A. Soffer,² W. H. Toki, R. J. Wilson, F. Winklmeier

Colorado State University, Fort Collins, Colorado 80523, USA

D. D. Altenburg, E. Feltresi, A. Hauke, H. Jasper, J. Merkel, A. Petzold, B. Spaan, K. Wacker

Universität Dortmund, Institut für Physik, D-44221 Dortmund, Germany

V. Klose, M. J. Kobel, H. M. Lacker, W. F. Mader, R. Nogowski, J. Schubert, K. R. Schubert, R. Schwierz,
J. E. Sundermann, A. Volk

Technische Universität Dresden, Institut für Kern- und Teilchenphysik, D-01062 Dresden, Germany

D. Bernard, G. R. Bonneaud, E. Latour, V. Lombardo, Ch. Thiebaux, M. Verderi

Laboratoire Leprince-Ringuet, CNRS/IN2P3, Ecole Polytechnique, F-91128 Palaiseau, France

P. J. Clark, W. Gradl, F. Muheim, S. Playfer, A. I. Robertson, J. E. Watson, Y. Xie

University of Edinburgh, Edinburgh EH9 3JZ, United Kingdom

M. Andreotti, D. Bettoni, C. Bozzi, R. Calabrese, A. Cecchi, G. Cibinetto, P. Franchini, E. Luppi,
M. Negrini, A. Petrella, L. Piemontese, E. Prencipe, V. Santoro

Università di Ferrara, Dipartimento di Fisica and INFN, I-44100 Ferrara, Italy

F. Anulli, R. Baldini-Ferroli, A. Calcaterra, R. de Sangro, G. Finocchiaro, S. Pacetti, P. Patteri,
I. M. Peruzzi,³ M. Piccolo, M. Rama, A. Zallo

Laboratori Nazionali di Frascati dell'INFN, I-00044 Frascati, Italy

A. Buzzo, R. Contri, M. Lo Vetere, M. M. Macri, M. R. Monge, S. Passaggio, C. Patrignani, E. Robutti,
A. Santroni, S. Tosi

Università di Genova, Dipartimento di Fisica and INFN, I-16146 Genova, Italy

²Now at Tel Aviv University, Tel Aviv, 69978, Israel

³Also with Università di Perugia, Dipartimento di Fisica, Perugia, Italy

K. S. Chaisanguanthum, M. Morii, J. Wu
Harvard University, Cambridge, Massachusetts 02138, USA

R. S. Dubitzky, J. Marks, S. Schenk, U. Uwer
Universität Heidelberg, Physikalisches Institut, Philosophenweg 12, D-69120 Heidelberg, Germany

D. J. Bard, P. D. Dauncey, R. L. Flack, J. A. Nash, W. Panduro Vazquez, M. Tibbetts
Imperial College London, London, SW7 2AZ, United Kingdom

P. K. Behera, X. Chai, M. J. Charles, U. Mallik
University of Iowa, Iowa City, Iowa 52242, USA

J. Cochran, H. B. Crawley, L. Dong, V. Eyges, W. T. Meyer, S. Prell, E. I. Rosenberg, A. E. Rubin
Iowa State University, Ames, Iowa 50011-3160, USA

Y. Y. Gao, A. V. Gritsan, Z. J. Guo, C. K. Lae
Johns Hopkins University, Baltimore, Maryland 21218, USA

A. G. Denig, M. Fritsch, G. Schott
Universität Karlsruhe, Institut für Experimentelle Kernphysik, D-76021 Karlsruhe, Germany

N. Arnaud, J. Béquilleux, A. D’Orazio, M. Davier, G. Grosdidier, A. Höcker, V. Lepeltier, F. Le Diberder,
A. M. Lutz, S. Pruvot, S. Rodier, P. Roudeau, M. H. Schune, J. Serrano, V. Sordini, A. Stocchi, L. Wang,
W. F. Wang, G. Wormser

*Laboratoire de l’Accélérateur Linéaire, IN2P3/CNRS et Université Paris-Sud 11, Centre Scientifique
d’Orsay, B. P. 34, F-91898 ORSAY Cedex, France*

D. J. Lange, D. M. Wright
Lawrence Livermore National Laboratory, Livermore, California 94550, USA

I. Bingham, J. P. Burke, C. A. Chavez, J. R. Fry, E. Gabathuler, R. Gamet, D. E. Hutchcroft, D. J. Payne,
K. C. Schofield, C. Touramanis

University of Liverpool, Liverpool L69 7ZE, United Kingdom

A. J. Bevan, K. A. George, F. Di Lodovico, R. Sacco, M. Sigamani
Queen Mary, University of London, E1 4NS, United Kingdom

G. Cowan, H. U. Flaecher, D. A. Hopkins, S. Paramesvaran, F. Salvatore, A. C. Wren
*University of London, Royal Holloway and Bedford New College, Egham, Surrey TW20 0EX, United
Kingdom*

D. N. Brown, C. L. Davis
University of Louisville, Louisville, Kentucky 40292, USA

J. Allison, N. R. Barlow, R. J. Barlow, Y. M. Chia, C. L. Edgar, G. D. Lafferty, T. J. West, J. I. Yi
University of Manchester, Manchester M13 9PL, United Kingdom

J. Anderson, C. Chen, A. Jawahery, D. A. Roberts, G. Simi, J. M. Tuggle
University of Maryland, College Park, Maryland 20742, USA

G. Blaylock, C. Dallapiccola, S. S. Hertzbach, X. Li, T. B. Moore, E. Salvati, S. Saremi
University of Massachusetts, Amherst, Massachusetts 01003, USA

R. Cowan, D. Dujmic, P. H. Fisher, K. Koenke, G. Sciolla, M. Spitznagel, F. Taylor, R. K. Yamamoto,
M. Zhao, Y. Zheng
*Massachusetts Institute of Technology, Laboratory for Nuclear Science, Cambridge, Massachusetts 02139,
USA*

S. E. Mclachlin,¹ P. M. Patel, S. H. Robertson
McGill University, Montréal, Québec, Canada H3A 2T8

A. Lazzaro, F. Palombo
Università di Milano, Dipartimento di Fisica and INFN, I-20133 Milano, Italy

J. M. Bauer, L. Cremaldi, V. Eschenburg, R. Godang, R. Kroeger, D. A. Sanders, D. J. Summers,
H. W. Zhao
University of Mississippi, University, Mississippi 38677, USA

S. Brunet, D. Côté, M. Simard, P. Taras, F. B. Viaud
Université de Montréal, Physique des Particules, Montréal, Québec, Canada H3C 3J7

H. Nicholson
Mount Holyoke College, South Hadley, Massachusetts 01075, USA

G. De Nardo, F. Fabozzi,⁴ L. Lista, D. Monorchio, C. Sciacca
Università di Napoli Federico II, Dipartimento di Scienze Fisiche and INFN, I-80126, Napoli, Italy

M. A. Baak, G. Raven, H. L. Snoek
*NIKHEF, National Institute for Nuclear Physics and High Energy Physics, NL-1009 DB Amsterdam, The
Netherlands*

C. P. Jessop, K. J. Knoepfel, J. M. LoSecco
University of Notre Dame, Notre Dame, Indiana 46556, USA

G. Benelli, L. A. Corwin, K. Honscheid, H. Kagan, R. Kass, J. P. Morris, A. M. Rahimi,
J. J. Regensburger, S. J. Sekula, Q. K. Wong
Ohio State University, Columbus, Ohio 43210, USA

N. L. Blount, J. Brau, R. Frey, O. Igonkina, J. A. Kolb, M. Lu, R. Rahmat, N. B. Sinev, D. Strom,
J. Strube, E. Torrence
University of Oregon, Eugene, Oregon 97403, USA

N. Gagliardi, A. Gaz, M. Margoni, M. Morandin, A. Pompili, M. Posocco, M. Rotondo, F. Simonetto,
R. Stroili, C. Voci
Università di Padova, Dipartimento di Fisica and INFN, I-35131 Padova, Italy

E. Ben-Haim, H. Briand, G. Calderini, J. Chauveau, P. David, L. Del Buono, Ch. de la Vaissière,
O. Hamon, Ph. Leruste, J. Malcès, J. Ocariz, A. Perez, J. Prendki
*Laboratoire de Physique Nucléaire et de Hautes Energies, IN2P3/CNRS, Université Pierre et Marie
Curie-Paris6, Université Denis Diderot-Paris7, F-75252 Paris, France*

⁴Also with Università della Basilicata, Potenza, Italy

L. Gladney

University of Pennsylvania, Philadelphia, Pennsylvania 19104, USA

M. Biasini, R. Covarelli, E. Manoni

Università di Perugia, Dipartimento di Fisica and INFN, I-06100 Perugia, Italy

C. Angelini, G. Batignani, S. Bettarini, M. Carpinelli,⁵ R. Cenci, A. Cervelli, F. Forti, M. A. Giorgi,
A. Lusiani, G. Marchiori, M. A. Mazur, M. Morganti, N. Neri, E. Paoloni, G. Rizzo, J. J. Walsh

Università di Pisa, Dipartimento di Fisica, Scuola Normale Superiore and INFN, I-56127 Pisa, Italy

J. Biesiada, P. Elmer, Y. P. Lau, C. Lu, J. Olsen, A. J. S. Smith, A. V. Telnov

Princeton University, Princeton, New Jersey 08544, USA

E. Baracchini, F. Bellini, G. Cavoto, D. del Re, E. Di Marco, R. Faccini, F. Ferrarotto, F. Ferroni,
M. Gaspero, P. D. Jackson, L. Li Gioi, M. A. Mazzoni, S. Morganti, G. Piredda, F. Polci, F. Renga,
C. Voena

Università di Roma La Sapienza, Dipartimento di Fisica and INFN, I-00185 Roma, Italy

M. Ebert, T. Hartmann, H. Schröder, R. Waldi

Universität Rostock, D-18051 Rostock, Germany

T. Adye, G. Castelli, B. Franek, E. O. Olaiya, W. Roethel, F. F. Wilson

Rutherford Appleton Laboratory, Chilton, Didcot, Oxon, OX11 0QX, United Kingdom

S. Emery, M. Escalier, A. Gaidot, S. F. Ganzhur, G. Hamel de Monchenault, W. Kozanecki, G. Vasseur,
Ch. Yèche, M. Zito

DSM/Daphnia, CEA/Saclay, F-91191 Gif-sur-Yvette, France

X. R. Chen, H. Liu, W. Park, M. V. Purohit, R. M. White, J. R. Wilson,

University of South Carolina, Columbia, South Carolina 29208, USA

M. T. Allen, D. Aston, R. Bartoldus, P. Bechtle, R. Claus, J. P. Coleman, M. R. Convery, J. C. Dingfelder,
J. Dorfan, G. P. Dubois-Felsmann, W. Dunwoodie, R. C. Field, T. Glanzman, S. J. Gowdy, M. T. Graham,
P. Grenier, C. Hast, W. R. Innes, J. Kaminski, M. H. Kelsey, H. Kim, P. Kim, M. L. Kocian,
D. W. G. S. Leith, S. Li, S. Luitz, V. Luth, H. L. Lynch, D. B. MacFarlane, H. Marsiske, R. Messner,
D. R. Muller, S. Nelson, C. P. O'Grady, I. Ofte, A. Perazzo, M. Perl, T. Pulliam, B. N. Ratcliff,
A. Roodman, A. A. Salnikov, R. H. Schindler, J. Schwiening, A. Snyder, D. Su, S. Sun, M. K. Sullivan,
K. Suzuki, S. K. Swain, J. M. Thompson, J. Va'vra, A. P. Wagner, M. Weaver, W. J. Wisniewski,
M. Wittgen, D. H. Wright, A. K. Yarritu, K. Yi, C. C. Young, V. Ziegler

Stanford Linear Accelerator Center, Stanford, California 94309, USA

P. R. Burchat, A. J. Edwards, S. A. Majewski, T. S. Miyashita, B. A. Petersen, L. Wilden

Stanford University, Stanford, California 94305-4060, USA

S. Ahmed, M. S. Alam, R. Bula, J. A. Ernst, V. Jain, B. Pan, M. A. Saeed, F. R. Wappler, S. B. Zain

State University of New York, Albany, New York 12222, USA

M. Krishnamurthy, S. M. Spanier, B. J. Wogslund

University of Tennessee, Knoxville, Tennessee 37996, USA

⁵Also with Università di Sassari, Sassari, Italy

R. Eckmann, J. L. Ritchie, A. M. Ruland, C. J. Schilling, R. F. Schwitters
University of Texas at Austin, Austin, Texas 78712, USA

J. M. Izen, X. C. Lou, S. Ye
University of Texas at Dallas, Richardson, Texas 75083, USA

F. Bianchi, F. Gallo, D. Gamba, M. Pelliccioni
Università di Torino, Dipartimento di Fisica Sperimentale and INFN, I-10125 Torino, Italy

M. Bomben, L. Bosisio, C. Cartaro, F. Cossutti, G. Della Ricca, L. Lanceri, L. Vitale
Università di Trieste, Dipartimento di Fisica and INFN, I-34127 Trieste, Italy

V. Azzolini, N. Lopez-March, F. Martinez-Vidal,⁶ D. A. Milanes, A. Oyanguren
IFIC, Universitat de Valencia-CSIC, E-46071 Valencia, Spain

J. Albert, Sw. Banerjee, B. Bhuyan, K. Hamano, R. Kowalewski, I. M. Nugent, J. M. Roney, R. J. Sobie
University of Victoria, Victoria, British Columbia, Canada V8W 3P6

P. F. Harrison, J. Ilic, T. E. Latham, G. B. Mohanty
Department of Physics, University of Warwick, Coventry CV4 7AL, United Kingdom

H. R. Band, X. Chen, S. Dasu, K. T. Flood, J. J. Hollar, P. E. Kutter, Y. Pan, M. Pierini, R. Prepost,
S. L. Wu
University of Wisconsin, Madison, Wisconsin 53706, USA

H. Neal
Yale University, New Haven, Connecticut 06511, USA

⁶Also with Universitat de Barcelona, Facultat de Fisica, Departament ECM, E-08028 Barcelona, Spain

1 INTRODUCTION

The Cabibbo-Kobayashi-Maskawa (CKM) mechanism [1, 2] for quark mixing describes all transitions between quarks in terms of only four parameters: three real rotation angles and one irreducible phase. Consequently, the flavor sector of the Standard Model (SM) is highly predictive. One particularly interesting prediction is that mixing-induced CP asymmetries in decays governed by $b \rightarrow q\bar{q}s$ ($q = u, d, s$) transitions are, to a good approximation, the same as those found in $b \rightarrow c\bar{c}s$ transitions. Since flavor changing neutral currents are forbidden at tree-level in the Standard Model, the $b \rightarrow s$ transition proceeds via loop diagrams (penguins), which are affected by new particles in many extensions of the SM.

Recently, various different $b \rightarrow s$ dominated charmless hadronic B decays have been studied in order to probe this prediction. The values of the mixing-induced CP asymmetry measured for each (quasi-)two-body mode can be compared to that measured in $b \rightarrow c\bar{c}s$ transitions (typically using $B^0 \rightarrow J/\psi K_S^0$). A recent compilation [3] of these results shows that they tend to have central values below that for $b \rightarrow c\bar{c}s$. However, there is currently no convincing evidence for new physics effects in these transitions. The most recent theoretical evaluations [4, 5, 6, 7, 8, 9, 10, 11, 12] suggest that SM corrections to the $b \rightarrow q\bar{q}s$ mixing-induced CP violation parameters should be small (in particular for the modes ϕK^0 , $\eta' K^0$ and $K_S^0 K_S^0 K_S^0$), and tend to *increase* the values (*i.e.* the opposite trend to that seen in the data). Clearly, more precise experimental results are required.

The compilation given in [3] includes several three-body modes, which may be used either by virtue of being CP eigenstates ($K_S^0 K_S^0 K_S^0$, $K_S^0 \pi^0 \pi^0$) [13] or since their CP content can be determined experimentally ($K^+ K^- K^0$) [14, 15]. It also includes quasi-two-body (Q2B) modes, such as $f_0(980) K_S^0$ and $\rho^0(770) K_S^0$, which are reconstructed via three-body final states ($K_S^0 \pi^+ \pi^-$ for these modes). For these channels, the precision of the Q2B approach is limited as other structures in the phase space may cause interference with the resonances considered as signal. Therefore, more precise results can be obtained using a full, time-dependent Dalitz plot (DP) fit of $B^0 \rightarrow K_S^0 \pi^+ \pi^-$. Furthermore the interference terms allow the cosine of the effective weak phase difference in mixing and decay to be determined, helping to resolve ambiguities which arise from the Q2B analysis. This approach has recently been successfully used in a time-dependent Dalitz plot analysis of $B^0 \rightarrow K^+ K^- K^0$ [15].

The discussion above assumes that the $b \rightarrow s$ penguin amplitude dominates the decay. However, for each mode contributing to the $K_S^0 \pi^+ \pi^-$ final state, there is also the possibility of a $b \rightarrow u$ tree diagram. These are doubly CKM suppressed compared to the $b \rightarrow s$ penguin (the tree is $\mathcal{O}(\lambda^4)$ whereas the penguin is $\mathcal{O}(\lambda^2)$, where λ is the usual Wolfenstein parameter [16, 17]). However, hadronic factors may result in a relative enhancement and hence significant “tree pollution”. The relative magnitudes of the tree and penguin amplitudes, $|T/P|$, thus can be different for each Q2B state, as can the strong phase difference. However, the relative weak phase between them is of course the same – and in the Standard Model is approximately equal to γ . An amplitude analysis, in contrast to a Q2B analysis, yields sufficient information to extract relative phases and magnitudes. DP analysis of $B^0 \rightarrow K_S^0 \pi^+ \pi^-$ (and similar modes) can therefore be used to determine γ [18, 19, 20, 21]. A comparison of the value obtained with that extracted from tree-level $B \rightarrow DK$ decays provides a SM test.

No results on time-dependent DP analysis of $B^0 \rightarrow K_S^0 \pi^+ \pi^-$ have yet been published. Belle have presented results of an analysis using 388 million $B\bar{B}$ pairs [22], which does not take into account either time-dependence or flavour-tag dependence. The results of the Belle analysis are

consistent with other studies of the $B^0 \rightarrow K_S^0 \pi^+ \pi^-$ decay [14, 23], as well as with measurements obtained from other $K\pi\pi$ systems: $K^+ \pi^- \pi^0$ [24, 25] and $K^+ \pi^+ \pi^-$ [26, 27]. The latter results indicate evidence for direct CP violation in the $B^+ \rightarrow \rho^0 K^+$ channel. If confirmed, this will be the first observation of CP violation in the decay of any charged particle. Taken together with the observation of direct CP violation in $B^0 \rightarrow K^+ \pi^-$ decays [28, 29], these results suggest that large CP violation effects are possible in $B^0 \rightarrow K^{*+} \pi^-$ (although current measurements of the effect are consistent with zero [23]).

In this paper we present preliminary results from the first time-dependent Dalitz plot analysis of the $B^0 \rightarrow K_S^0 \pi^+ \pi^-$ decay. In Section 2 we describe the time-dependent Dalitz plot formalism, and introduce the signal parameters that are extracted in our fit to data. In Section 3 we briefly describe the *BABAR* detector and the data set. In Section 4, we explain the selection requirements used to obtain our signal candidates and suppress backgrounds. In the same section we describe the methods used to control experimental effects such as resolution in the fit to data. In Section 5 we present the results of the fit, and extract parameters relevant to the contributing Q2B decays. In Section 6 we discuss systematic uncertainties in our results, and finally we summarize our results in Section 7.

2 ANALYSIS OVERVIEW

Using a maximum-likelihood fit, we measure relative phases and magnitudes for the different resonant decay modes, taking advantage of the interference between them in the Dalitz plot. Below we detail the formalism used in the present analysis.

2.1 DECAY AMPLITUDES

We consider the decay of a spin-zero B^0 with four-momentum p_B into the three daughters π^+ , π^- and K_S^0 with p_+ , p_- and p_0 , their corresponding four-momenta. Using as independent (Mandelstam) variables the invariant squared masses

$$s_+ = (p_+ + p_0)^2, \quad s_- = (p_- + p_0)^2, \quad (1)$$

the invariant squared mass of the positive and negative pion, $s_0 = (p_+ + p_-)^2$, is obtained from energy and momentum conservation

$$s_0 = m_{B^0}^2 + 2m_{\pi^+}^2 + m_{K_S^0}^2 - s_+ - s_- . \quad (2)$$

The differential B^0 decay width with respect to the variables defined in Equation (1) (*i.e.* the *Dalitz plot*) reads

$$d\Gamma(B^0 \rightarrow K_S^0 \pi^+ \pi^-) = \frac{1}{(2\pi)^3} \frac{|\mathcal{A}|^2}{32m_{B^0}^3} ds_+ ds_- , \quad (3)$$

where \mathcal{A} is the Lorentz-invariant amplitude of the three-body decay. In the following, the amplitudes \mathcal{A} and its CP conjugate $\bar{\mathcal{A}}$ correspond to the transitions $B^0 \rightarrow K_S^0 \pi^+ \pi^-$ and $\bar{B}^0 \rightarrow K_S^0 \pi^+ \pi^-$, respectively. We describe the distribution of signal events in the DP using an isobar approximation, which models the total amplitude as resulting from a sum of amplitudes from the individual decay

channels

$$\mathcal{A}(s_+, s_-) = \sum_{j=1}^N c_j F_j(s_+, s_-) \quad (4)$$

$$\overline{\mathcal{A}}(s_+, s_-) = \sum_{j=1}^N \overline{c}_j \overline{F}_j(s_+, s_-) \quad (5)$$

where F_j are DP dependent dynamical amplitudes described in the following, and c_j are complex coefficients describing the relative magnitude and phase of the different decay channels. All the weak phase dependence is contained in c_j , and F_j contains strong dynamics only, therefore

$$F_j(s_+, s_-) = \overline{F}_j(s_-, s_+) . \quad (6)$$

The resonance dynamics are contained within the F_j terms, which are represented by the product of the invariant mass and angular distribution probabilities, *i.e.*

$$F_j^L(s_+, s_-) = R_j(m) \times X_L(|\vec{p}^*| r) \times X_L(|\vec{q}| r) \times T_j(L, \vec{p}, \vec{q}) , \quad (7)$$

where

- m is the invariant mass of the decay products of the resonance,
- $R_j(m)$ is the resonance mass term or “lineshape” (e.g. Breit–Wigner),
- X_L are Blatt–Weisskopf barrier factors [30] with parameter r . These factors are taken to be unity in the present analysis, both in Equation (7) and in the lineshapes. The effect of this choice is accounted for as a systematic uncertainty.
- \vec{p}^* is the momentum of the bachelor particle evaluated in the rest frame of the B ,
- \vec{p} and \vec{q} are the momenta of the bachelor particle and one of the resonance daughters respectively, both evaluated in the rest frame of the resonance,
- L is the orbital angular momentum between the resonance and the bachelor, and
- $T_j(L, \vec{p}, \vec{q})$ is the angular distribution, where:

$$L = 0 \quad : \quad T_j = 1 , \quad (8)$$

$$L = 1 \quad : \quad T_j = -4\vec{p} \cdot \vec{q} , \quad (9)$$

$$L = 2 \quad : \quad T_j = \frac{8}{3} [3(\vec{p} \cdot \vec{q})^2 - (|\vec{p}||\vec{q}|)^2] . \quad (10)$$

The lineshape differs for each component included in the fit. The lineshapes used are Relativistic Breit–Wigner (RBW) [31], Flatté [32], Gounaris-Sakurai (GS) [33] and LASS [26, 34, 35]. A flat phase space term has been included in the signal model to account for nonresonant (NR) $B^0 \rightarrow K_S^0 \pi^+ \pi^-$ decays. The components of the signal model are summarized in Table 1.

Resonance	Parameters	Form Factor	Ref. for Parameters
f_0	mass = 965 ± 10 $g_\pi = 165 \pm 18$ $g_K = 695 \pm 93$	Flatté	[36]
ρ^0	mass = 775.5 ± 0.4 width = 146.4 ± 1.1	GS	[31]
$K^{*+}(892)$ $K^{*-}(892)$	mass = 891.66 ± 0.26 width = 50.8 ± 0.9	RBW	[31]
$K^{*+}(1430)$ $K^{*-}(1430)$	mass = 1415 ± 3 width = 300 ± 6 cutoff = 2000 $a = 2.07 \pm 0.1$ (GeV $^{-1}$) $r = 3.32 \pm 0.34$ (GeV $^{-1}$)	LASS	[26, 37]
$f_X(1300)$	mass = 1449 ± 13 width = 126 ± 25	RBW	[22]
$f_2(1270)$	mass = 1275.4 ± 1.1 width = $185.2^{+3.1}_{-2.5}$	RBW	[31]
$\chi_{c0}(1P)$	mass = 3414.75 ± 0.35 width = 10.4 ± 0.7	RBW	[31]
NR decays		flat phase space	

Table 1: *Parameters of the DP model used in the fit. Values are given in MeV, unless mentioned otherwise.*

2.2 TIME DEPENDENCE

With $\Delta t \equiv t_{\text{sig}} - t_{\text{tag}}$ defined as the proper time interval between the decay of the fully reconstructed $B^0 \rightarrow K_S^0 \pi^+ \pi^-$ (B_{sig}^0) and that of the other meson (B_{tag}^0) from the $\Upsilon(4S)$, the time-dependent decay rate $|\mathcal{A}_{\text{sig}}^+(\Delta t)|^2$ ($|\mathcal{A}_{\text{sig}}^-(\Delta t)|^2$) when the B_{tag}^0 is a B^0 (\bar{B}^0) is given by

$$\begin{aligned}
|\mathcal{A}_{\text{sig}}^\pm(\Delta t)|^2 &= \frac{e^{-|\Delta t|/\tau_{B^0}}}{4\tau_{B^0}} \left[|\mathcal{A}|^2 + |\bar{\mathcal{A}}|^2 \right. \\
&\quad \mp (|\mathcal{A}|^2 - |\bar{\mathcal{A}}|^2) \cos(\Delta m_d \Delta t) \\
&\quad \left. \pm 2\text{Im} [\bar{\mathcal{A}}\mathcal{A}^*] \sin(\Delta m_d \Delta t) \right], \tag{11}
\end{aligned}$$

where τ_{B^0} is the neutral B meson lifetime and Δm_d is the $B^0\bar{B}^0$ mass difference. In the last formula and in the following, the DP dependence of amplitudes is implicit. Here, we have assumed that there is no CP violation in mixing, and have used a convention whereby the phase from $B^0\bar{B}^0$ mixing is absorbed into the \bar{B}^0 decay amplitude¹ (*i.e.* into the \bar{c}_j terms). Lifetime differences in the neutral B meson system are assumed to be negligible.

¹In other terms, we assume that $|q/p| = 1$ and absorb q/p into \bar{c}_j .

2.3 THE SQUARE DALITZ PLOT

Both the signal events and the combinatorial $e^+e^- \rightarrow q\bar{q}$ ($q = u, d, s, c$) continuum background events populate the kinematic boundaries of the DP due to the low final state masses compared with the B^0 mass. We find the representation in Equation (3) is inconvenient when one wants to use empirical reference shapes in a maximum-likelihood fit. Large variations occurring in small areas of the DP are very difficult to describe in detail. We therefore apply the transformation

$$ds_+ ds_- \longrightarrow |\det J| dm' d\theta', \quad (12)$$

which defines the *Square Dalitz plot* (SDP). The new coordinates are

$$m' \equiv \frac{1}{\pi} \arccos \left(2 \frac{m_0 - m_0^{\min}}{m_0^{\max} - m_0^{\min}} - 1 \right), \quad \theta' \equiv \frac{1}{\pi} \theta_0, \quad (13)$$

where $m_0 = \sqrt{s_0}$ is the $\pi^+\pi^-$ invariant mass, $m_0^{\max} = m_{B^0} - m_{K_S^0}$ and $m_0^{\min} = 2m_{\pi^+}$ are the kinematic limits of m_0 , θ_0 is the $\pi^+\pi^-$ resonance helicity angle, defined as the angle between the π^- and the K_S^0 in the $\pi^+\pi^-$ rest frame, and J is the Jacobian of the transformation. Both variables range between 0 and 1. The determinant of the Jacobian is given by

$$|\det J| = 4 |\mathbf{p}_+^*| |\mathbf{p}_0^*| m_0 \cdot \frac{\partial m_0}{\partial m'} \cdot \frac{\partial \cos \theta_0}{\partial \theta'}, \quad (14)$$

where $|\mathbf{p}_+^*| = \sqrt{E_+^{*2} - m_{\pi^+}^2}$ and $|\mathbf{p}_0^*| = \sqrt{E_0^{*2} - m_{K_S^0}^2}$, and where the π^+ (K_S^0) energy E_+^* (E_0^*), is defined in the $\pi^+\pi^-$ rest frame. This same transformation has been used in previous B decay DP analyses, *e.g.* Ref. [38].

3 THE BABAR DETECTOR AND DATASET

The data used in this analysis were collected with the *BABAR* detector at the PEP-II asymmetric-energy e^+e^- storage ring at SLAC between October 1999 and August 2006. The sample consists of about 347 fb^{-1} , corresponding to $(383 \pm 3) \times 10^6 B\bar{B}$ pairs collected at the $\Upsilon(4S)$ resonance (“on-resonance”), and an integrated luminosity of 36.6 fb^{-1} collected about 40 MeV below the $\Upsilon(4S)$ (“off-resonance”).

A detailed description of the *BABAR* detector is presented in Ref. [39]. The tracking system used for track and vertex reconstruction has two components: a silicon vertex tracker (SVT) and a drift chamber (DCH), both operating within a 1.5 T magnetic field generated by a superconducting solenoidal magnet. Photons are identified in an electromagnetic calorimeter (EMC) surrounding a detector of internally reflected Cherenkov light (DIRC), which associates Cherenkov photons with tracks for particle identification (PID). Muon candidates are identified with the use of the instrumented flux return (IFR) of the solenoid.

4 EVENT SELECTION AND BACKGROUND SUPPRESSION

We reconstruct $B^0 \rightarrow K_S^0 \pi^+ \pi^-$ candidates from pairs of oppositely-charged tracks and a $K_S^0 \rightarrow \pi^+ \pi^-$ candidate, which are required to form a good quality vertex. In order to ensure that all events are within the DP boundaries, we constrain the invariant mass of the final state to the B

mass. For the $\pi^+\pi^-$ pair from the B , we use information from the tracking system, EMC, and DIRC to remove tracks consistent with electron, kaon and proton hypotheses. In addition, we require at least one track to be inconsistent with the muon hypothesis based on information from the IFR. The K_S^0 candidate is required to have a mass within $15 \text{ MeV}/c^2$ of the nominal K^0 mass [31] and a decay vertex well separated from the B^0 decay vertex. In addition, the cosine of the angle between the K_S^0 flight direction and the vector between the B -daughter pions and the K_S^0 vertices must be greater than 0.999.

A B -meson candidate is characterized kinematically by the energy-substituted mass $m_{\text{ES}} \equiv \sqrt{(s/2 + \mathbf{p}_i \cdot \mathbf{p}_B)^2/E_i^2 - \mathbf{p}_B^2}$ and energy difference $\Delta E \equiv E_B^* - \frac{1}{2}\sqrt{s}$, where (E_B, \mathbf{p}_B) and (E_i, \mathbf{p}_i) are the four-vectors of the B -candidate and the initial electron-positron system, respectively. The asterisk denotes the $\Upsilon(4S)$ frame, and s is the square of the invariant mass of the electron-positron system. We require $5.272 < m_{\text{ES}} < 5.286 \text{ GeV}/c^2$ and $|\Delta E| < 0.065 \text{ GeV}$.

Backgrounds arise primarily from random combinations in continuum events. To enhance discrimination between signal and continuum, we use a neural network (NN) [40] to combine four discriminating variables: the angles with respect to the beam axis of the B momentum and B thrust axis in the $\Upsilon(4S)$ frame; and the zeroth and second order monomials $L_{0,2}$ of the energy flow about the B thrust axis. The monomials are defined by $L_n = \sum_i \mathbf{p}_i \times |\cos \theta_i|^n$, where θ_i is the angle with respect to the B thrust axis of track or neutral cluster i , \mathbf{p}_i is its momentum, and the sum excludes the B candidate. The NN is trained using off-resonance data as well as simulated signal events that passed the selection criteria. The final sample of signal candidates is selected with a requirement on the NN output that retains 90% (29%) of the signal (continuum).

The time difference Δt is obtained from the measured distance between the z positions (along the beam direction) of the B_{sig}^0 and B_{tag}^0 decay vertices, and the boost $\beta\gamma = 0.56$ of the e^+e^- system: $\Delta t = \Delta z/\beta\gamma c$. B^0 candidates with $|\Delta t| > 20 \text{ ps}$ are rejected, as well as candidates for which the error on Δt is higher than 2.5 ps. To determine the flavor of the B_{tag}^0 we use the B flavor tagging algorithm of Ref. [41]. This produces six mutually exclusive tagging categories. We also retain untagged events in a seventh category to improve the efficiency of the signal selection and because these events contribute to the measurement of direct CP violation [42]. Events with multiple B candidates passing the full selection occur between $\sim 1\%$ of the time for nonresonant signal and $\sim 8\%$ of the time for $B^0 \rightarrow f_0(980)K_S^0$ signal. If an event has more than one candidate, we select one using an arbitrary but reproducible procedure based on the event timestamp.

With the above selection criteria, we obtain a signal efficiency determined from Monte Carlo (MC) simulation of 21 – 25% depending on the composition of the DP.

Of the selected signal events, 8% of $B^0 \rightarrow \rho^0 K_S^0$, 6% of $B^0 \rightarrow K^*(892)^+\pi^-$ and 4% of $B^0 \rightarrow f_0(980)K_S^0$ events are misreconstructed. Misreconstructed events occur when a track from the tagging B is assigned to the reconstructed signal candidate. This occurs most often for low-momentum tracks and hence the misreconstructed events are concentrated in the corners of the DP. Since these are also the areas where the low-mass resonances overlap strongly with other resonances, it is important to model the misreconstructed events correctly. The details of the model for misreconstructed events over the DP is detailed in Section 4.2.1.

4.1 BACKGROUND FROM OTHER B DECAYS

We use MC simulated events to study the background from other B decays. More than fifty channels were considered in preliminary studies, of which twenty are included in the final likelihood model – decays with at least two events expected after selection. These exclusive B background modes

Mode	Varied	BR	Number of events
$B^0 \rightarrow D^- (\rightarrow K_S^0 \pi^-) \pi^+$	yes	–	3377 ± 60
$B^0 \rightarrow J/\psi (\rightarrow l^+ l^-) K_S^0$	yes	–	1803 ± 43
$B^0 \rightarrow \psi(2S) K_S^0$	yes	–	142 ± 13
$B^0 \rightarrow \eta' K_S^0$	yes	–	37 ± 16
$B^0 \rightarrow a_1^\pm \pi^\mp$	no	$(39.7 \pm 3.7) \times 10^{-6}$	7.3 ± 0.7
$B^0 \rightarrow D^{*-} (\rightarrow D\pi) \pi^+$	no	$(2.57 \pm 0.10) \times 10^{-3}$	43.8 ± 2.5
$B^0 \rightarrow D^- h^+ ; B^0 \rightarrow D^- \mu^+ \nu_\mu$	no	$(2.94 \pm 0.19) \times 10^{-3}$	281 ± 20
$B^0 \rightarrow D^{*-} \rho^+$	no	$(14.2 \pm 1.4) \times 10^{-3}$	34.5 ± 4.6
$B^0 \rightarrow \{\text{neutral generic decays}\}$	no	–	114 ± 7
$B^+ \rightarrow \{\text{charged generic decays}\}$	no	–	282 ± 11

Table 2: *Summary of B background modes taken into account for the likelihood model. When the yield is varied in the fit, the quoted number of events corresponds to the fit results. Otherwise the expected number, taking into account the branching ratios and efficiency, is given.*

are grouped into ten different classes that gather decays with similar kinematic and topological properties: nine for neutral B decays, one of which accounts for inclusive decays, and one for charged inclusive B decays.

Table 2 summarizes the ten background classes that are used in the fit. When the yield of a class is varied in the Maximum Likelihood fit the quoted number of events corresponds to the fit results. For the other modes, the expected number of selected events is computed by multiplying the selection efficiency (estimated using MC simulated decays) by the branching fraction, scaled to the dataset luminosity (347 fb^{-1}). The world average branching ratios [3, 31] have been used for the experimentally known decay modes.

4.2 THE MAXIMUM-LIKELIHOOD FIT

We perform an unbinned extended maximum-likelihood fit to extract the inclusive $B^0 \rightarrow K_S^0 \pi^+ \pi^-$ event yield and the resonant amplitudes. The fit uses the variables m_{ES} , ΔE , the NN output and the SDP to discriminate signal from background. The Δt measurement allows the determination of mixing-induced CP violation and provides additional continuum background rejection.

The selected on-resonance data sample is assumed to consist of signal, continuum background and B background components, separated by the flavor and tagging category of the tag side B decay. The signal likelihood consists of the sum of a correctly reconstructed (“truth-matched”, TM) component and a misreconstructed (“self-cross-feed”, SCF) component.

The probability density function (PDF) \mathcal{P}_i^c for an event i in tagging category c is the sum of

the probability densities of all components, namely

$$\begin{aligned}
\mathcal{P}_i^c &\equiv N_{\text{sig}} f_{\text{sig}}^c \left[(1 - \bar{f}_{\text{SCF}}^c) \mathcal{P}_{\text{sig-TM},i}^c + \bar{f}_{\text{SCF}}^c \mathcal{P}_{\text{sig-SCF},i}^c \right] \\
&+ N_{q\bar{q}}^c \frac{1}{2} (1 + q_{\text{tag},i} A_{q\bar{q},\text{tag}}) \mathcal{P}_{q\bar{q},i}^c \\
&+ \sum_{j=1}^{N_{\text{class}}^{B^+}} N_{B^+j} f_{B^+j}^c \frac{1}{2} (1 + q_{\text{tag},i} A_{B^+,\text{tag},j}) \mathcal{P}_{B^+,ij}^c \\
&+ \sum_{j=1}^{N_{\text{class}}^{B^0}} N_{B^0j} f_{B^0j}^c \mathcal{P}_{B^0,ij}^c ,
\end{aligned} \tag{15}$$

where N_{sig} is the total number of $K_S^0 \pi^+ \pi^-$ signal events in the data sample; f_{sig}^c is the fraction of signal events that are tagged in category c ; \bar{f}_{SCF}^c is the fraction of SCF events in tagging category c , averaged over the DP; $\mathcal{P}_{\text{sig-TM},i}^c$ and $\mathcal{P}_{\text{sig-SCF},i}^c$ are the products of PDFs of the discriminating variables used in tagging category c for TM and SCF events, respectively; $N_{q\bar{q}}^c$ is the number of continuum events that are tagged in category c ; $q_{\text{tag},i}$ is the tag flavor of the event, defined to be +1 for a B_{tag}^0 and -1 for a \bar{B}_{tag}^0 ; $A_{q\bar{q},\text{tag}}$ parameterizes possible tag asymmetry in continuum events; $\mathcal{P}_{q\bar{q},i}^c$ is the continuum PDF for tagging category c ; $N_{\text{class}}^{B^+}$ ($N_{\text{class}}^{B^0}$) is the number of charged (neutral) B -related background classes considered in the fit, namely one (nine); N_{B^+j} (N_{B^0j}) is the number of expected events in the charged (neutral) B background class j ; $f_{B^+j}^c$ ($f_{B^0j}^c$) is the fraction of charged (neutral) B background events of class j that are tagged in category c ; $A_{B^+,\text{tag},j}$ describes a possible tag asymmetry in the charged B background class j ; $\mathcal{P}_{B^+,ij}^c$ is the B^+ background PDF for tagging category c and class j ; and $\mathcal{P}_{B^0,ij}^c$ is the neutral B background PDF for tagging category c and class j . Correlations between the tag and the position in the DP are absorbed in tag-flavor-dependent SDP PDFs that are used for charged B and continuum background. The PDFs \mathcal{P}_X^c ($X = \{\text{sig-TM}, \text{sig-SCF}, q\bar{q}, B^+, B^0\}$) are the product of the four PDFs of the discriminating variables², $x_1 = m_{\text{ES}}$, $x_2 = \Delta E$, $x_3 = \text{NN output}$ and the triplet $x_4 = \{m', \theta', \Delta t\}$:

$$\mathcal{P}_{X,i(j)}^c \equiv \prod_{k=1}^4 P_{X,i(j)}^c(x_k) , \tag{16}$$

where i is the event index and j is a B background class. The extended likelihood over all tagging categories is given by

$$\mathcal{L} \equiv \prod_{c=1}^7 e^{-\bar{N}^c} \prod_i^{N^c} \mathcal{P}_i^c , \tag{17}$$

where \bar{N}^c is the total number of events expected in category c .

A total of 75 parameters are varied in the fit. They include the 12 inclusive yields (signal, four B background classes and seven continuum yields, one per tagging category) and 30 parameters for the complex amplitudes from Equation (11). Most of the parameters describing the continuum distributions are free in the fit.

² Not all the PDFs depend on the tagging category. The general notations $P_{X,i(j)}^c$ and $\mathcal{P}_{X,i(j)}^c$ are used for simplicity.

4.2.1 THE Δt AND DALITZ PLOT PDFS

The SDP PDFs require as input the DP dependent relative selection efficiency, $\varepsilon = \varepsilon(m', \theta')$, and SCF fraction, $f_{\text{SCF}} = f_{\text{SCF}}(m', \theta')$. Both quantities are taken from MC simulation. Away from the DP corners the efficiency is uniform. It decreases when approaching the corners, where one of the three particles in the final state is close to rest so that the acceptance requirements on the particle reconstruction become restrictive. Combinatorial backgrounds and hence SCF fractions are large in the corners of the DP due to the presence of soft tracks.

For an event i , we define the time-dependent SDP PDFs

$$P_{\text{sig-TM},i}(m', \theta', \Delta t) = \varepsilon_i (1 - f_{\text{SCF},i}) |\det J_i| |\mathcal{A}^\pm(\Delta t)|^2, \quad (18)$$

$$P_{\text{sig-SCF},i}(m', \theta', \Delta t) = \varepsilon_i f_{\text{SCF},i} |\det J_i| |\mathcal{A}^\pm(\Delta t)|^2, \quad (19)$$

where $P_{\text{sig-TM},i}(m', \theta', \Delta t)$ and $P_{\text{sig-SCF},i}(m', \theta', \Delta t)$ are normalized. The phase space integration involves the expectation values $\langle \varepsilon (1 - f_{\text{SCF}}) | \det J | F_\kappa F_\sigma^* \rangle$ and $\langle \varepsilon f_{\text{SCF}} | \det J | F_\kappa F_\sigma^* \rangle$ for TM and SCF events, where the indices κ, σ run over all resonances belonging to the signal model. The expectation values are model-dependent and are computed with the use of MC integration over the SDP:

$$\langle \varepsilon (1 - f_{\text{SCF}}) | \det J | F_\kappa F_\sigma^* \rangle = \frac{\int_0^1 \int_0^1 \varepsilon (1 - f_{\text{SCF}}) | \det J | F_\kappa F_\sigma^* dm' d\theta'}{\int_0^1 \int_0^1 \varepsilon | \det J | F_\kappa F_\sigma^* dm' d\theta'} , \quad (20)$$

and similarly for $\langle \varepsilon f_{\text{SCF}} | \det J | F_\kappa F_\sigma^* \rangle$, where all quantities in the integrands are DP dependent.

Equation (15) invokes the phase space-averaged SCF fraction $\bar{f}_{\text{SCF}} \equiv \langle f_{\text{SCF}} | \det J | F_\kappa F_\sigma^* \rangle$. The PDF normalization is decay-dynamics-dependent and is computed iteratively. We determine the average SCF fractions separately for each tagging category from MC simulation.

The width of the dominant resonances is large compared to the mass resolution for TM events (about $8 \text{ MeV}/c^2$ core Gaussian resolution). We therefore neglect resolution effects in the TM model. Misreconstructed events have a poor mass resolution that strongly varies across the DP. It is described in the fit by a 2×2 -dimensional resolution function

$$R_{\text{SCF}}(m'_r, \theta'_r, m'_t, \theta'_t) , \quad (21)$$

which represents the probability to reconstruct at the coordinate (m'_r, θ'_r) an event that has the true coordinate (m'_t, θ'_t) . It obeys the unitarity condition

$$\int_0^1 \int_0^1 R_{\text{SCF}}(m'_r, \theta'_r, m'_t, \theta'_t) dm'_r d\theta'_r = 1 , \quad (22)$$

and is convolved with the signal model. The R_{SCF} function is obtained from MC simulation.

We use the signal model described in Section 2.1. It contains the dynamical information and is connected with Δt via the matrix element in Equation (11), which serves as the PDF. The PDF is diluted by the effects of mistagging and the limited vertex resolution [38]. The Δt resolution function for signal (both TM and SCF) and B background events is a sum of three Gaussian distributions, with parameters determined by a fit to fully reconstructed B^0 decays [41].

The SDP- and Δt -dependent PDFs factorize for the charged B background modes, but not necessarily for the neutral B background due to $B^0 \bar{B}^0$ mixing.

The charged B background contribution to the likelihood (Equation (15)) involves the parameter $A_{B^+, \text{tag}}$, multiplied by the tag flavor q_{tag} of the event. In the presence of significant tag-“charge” correlation (represented by an effective flavor-tag-versus-Dalitz-coordinate correlation), it parameterizes possible direct CP violation in these events. We use distinct SDP PDFs for each reconstructed B flavor tag, and a flavor-tag-averaged PDF for untagged events. The PDFs are obtained from MC simulation and are described by histograms. The Δt resolution parameters are determined by a fit to fully reconstructed B^+ decays. For the B^+ background class we adjust the effective lifetime to account for the misreconstruction of the event that modifies the nominal Δt resolution function.

The neutral B background is parameterized with PDFs that depend on the flavor tag of the event. In the case of CP eigenstates, correlations between the flavor tag and the Dalitz coordinate are expected to be small. However, non- CP eigenstates, such as $a_1^\pm \pi^\mp$, may exhibit such correlations. Both types of decays can have direct and mixing-induced CP violation. A third type of decay involves charged D mesons and does not exhibit mixing-induced CP violation, but usually has a strong correlation between the flavor tag and the DP coordinate (the D meson charge), because it consists of B -flavor eigenstates. Direct CP violation is also possible in these decays, though it is set to zero in the nominal model. The DP PDFs are obtained from MC simulation and are described by histograms. For neutral B background, the signal Δt resolution model is assumed.

The DP treatment of the continuum events is similar to that used for charged B background. The SDP PDF for continuum background is obtained from on-resonance events selected in the m_{ES} sidebands and corrected for feed-through from B decays. A large number of cross checks have been performed to ensure the high fidelity of the empirical shape used. Analytical models were found to be insufficient. The continuum Δt distribution is parameterized as the sum of three Gaussian distributions with common mean and three distinct widths that scale the Δt per-event error. This yields six shape parameters that are determined by the fit. The model is motivated by the observation that the Δt average is independent of its error, and that the Δt RMS depends linearly on the Δt error.

4.2.2 DESCRIPTION OF THE OTHER VARIABLES

The m_{ES} distribution of TM signal events is parameterized by a bifurcated Crystal Ball function [43, 44, 45], which is a combination of a one-sided Gaussian and a Crystal Ball function. The mean and two widths of this function are determined by the fit. A non-parametric function is used to describe the SCF signal component. The ΔE distribution of TM events is parameterized by a double Gaussian function. Misreconstructed events are described by a non-parametric function.

Both m_{ES} and ΔE PDFs are described by non-parametric functions for all B background classes. Exceptions to this are the m_{ES} PDFs for $B^0 \rightarrow D^- \pi^+$ and $B^0 \rightarrow J/\psi K_S^0$ components, and the ΔE PDF for $B^0 \rightarrow D^- \pi^+$, which are the same as the corresponding distributions of TM signal events.

The m_{ES} and ΔE PDFs for continuum events are parameterized with an ARGUS shape function [46] and a first-order polynomial, respectively, with parameters determined by the fit.

We use non-parametric functions to empirically describe the distributions of the NN output found in the MC simulation for TM and SCF signal events, and for B background events. We distinguish tagging categories for TM signal events to account for differences observed in the shapes.

The continuum NN distribution is parameterized by a third-order polynomial that is constrained to take positive values in the range populated by the data. The coefficients of the polynomial are determined by the fit. Continuum events exhibit a correlation between the DP coordinate and the

shape of the event that is exploited in the NN. To correct for residual effects, we introduce a linear dependence of the polynomial coefficients on the distance of the DP coordinate from the kinematic boundaries of the DP. The parameters describing this dependence are determined by the fit.

5 FIT RESULTS

The maximum-likelihood fit of 22525 candidates results in a $B^0 \rightarrow K_S^0 \pi^+ \pi^-$ event yield of 2172 ± 70 and a continuum yield of 14272 ± 126 , where the errors are statistical only. Figure 1 shows distributions of the likelihood ratio (signal/background) for all the events entering the fit and for the signal-like region. Figure 2 shows distributions of ΔE , m_{ES} , NN output, $\Delta t/\sigma(\Delta t)$, where $\sigma(\Delta t)$ is the per-event error on Δt , as well as the DP variables m' and θ' , which are enhanced in signal content by requirements on the signal-to-continuum likelihood ratios of the other discriminating variables. Figure 3 shows similar distributions for $m(K_S^0 \pi^+)$, $m(K_S^0 \pi^-)$ and $m(\pi^+ \pi^-)$. These distributions indicate the good quality of the fit. Signal enhanced distributions of Δt and Δt asymmetry for events in the regions of $f_0(980)K_S^0$ and $\rho^0(770)K_S^0$ are shown in Figure 4.

In the fit, we measure directly the relative magnitudes and phases of the different components of the signal model. The results are given together with their statistical errors in Table 3. The measured relative amplitudes c_σ , where the index represents an intermediate resonance, are used to extract the Q2B parameters, for which the definitions are given below.

Table 3: *Summary of fit results for the magnitudes $|c_\sigma|$ and phases ϕ in degrees of the resonant amplitudes. The quoted error is statistical only.*

Resonance Name	$ c_\sigma $	ϕ [degrees]	$ \bar{c}_\sigma $ ($ \bar{c}_\sigma $)	ϕ [degrees]
$f_0(980)K_S^0$	4.0	0.0	2.8 ± 0.7	-88.6 ± 21.3
$\rho^0(770)K_S^0$	0.10 ± 0.02	58.6 ± 16.4	0.09 ± 0.02	21.3 ± 21.2
$f_0(1300)K_S^0$	1.9 ± 0.4	117.6 ± 22.6	1.1 ± 0.3	-15.2 ± 23.8
Nonresonant	3.0 ± 0.6	13.8 ± 14.3	3.7 ± 0.5	-16.2 ± 17.3
$K^{*+}(892)\pi^-$	0.136 ± 0.021	-60.7 ± 18.5	0.113 ± 0.018	102.6 ± 22.9
$K^{*+}(1430)\pi^-$	4.9 ± 0.7	-82.4 ± 16.8	7.1 ± 0.9	79.2 ± 20.5
$f_2(1270)K_S^0$	0.011 ± 0.004	62.9 ± 23.3	0.010 ± 0.003	-73.9 ± 27.8
$\chi_{c0}(1P)K_S^0$	0.34 ± 0.15	68.7 ± 31.1	0.40 ± 0.11	154.5 ± 28.6

For a resonant decay mode σ which is a CP eigenstate, the following Q2B parameters are extracted: the angle $2\beta_{\text{eff}}$, defined as:

$$2\beta_{\text{eff}}(\sigma) = \arg(c_\sigma \bar{c}_\sigma^*) , \quad (23)$$

and the direct and mixing-induced CP asymmetries, defined as:

$$C(\sigma) = \frac{|c_\sigma|^2 - |\bar{c}_\sigma|^2}{|c_\sigma|^2 + |\bar{c}_\sigma|^2} , \quad (24)$$

$$S(\sigma) = \frac{2\mathcal{I}m(\bar{c}_\sigma c_\sigma^*)}{|c_\sigma|^2 + |\bar{c}_\sigma|^2} ; \quad (25)$$

for a self-tagging resonant decay mode σ such as $B^0 \rightarrow K^{*+}(892)\pi^-$, the direct CP asymmetry is defined as:

$$A_{CP}(\sigma) = \frac{|\bar{c}_\sigma|^2 - |c_\sigma|^2}{|\bar{c}_\sigma|^2 + |c_\sigma|^2}; \quad (26)$$

the relative isobar phase between two resonances, σ and κ is defined by

$$\Delta\phi(\sigma, \kappa) = \text{arg}(c_\sigma c_\kappa^*); \quad (27)$$

and the similar quantity for a self-tagging resonant decay mode, σ and its charge conjugate $\bar{\sigma}$ is:

$$\Delta\phi(\sigma, \bar{\sigma}) = \text{arg}(c_\sigma \bar{c}_\sigma^*); \quad (28)$$

recall that we use a convention in which the \bar{B}^0 decay amplitudes have absorbed the phase from $B^0\bar{B}^0$ mixing. Finally, we also extract the relative fraction f of a Q2B channel σ , which is calculated as:

$$f(\sigma) = \frac{(|c_\sigma|^2 + |\bar{c}_\sigma|^2)\langle F_\sigma F_\sigma^* \rangle}{\sum_{\mu\nu} (c_\mu c_\nu^* + \bar{c}_\mu \bar{c}_\nu^*)\langle F_\mu F_\nu^* \rangle}, \quad (29)$$

where

$$\langle F_\mu F_\nu^* \rangle = \int F_\mu F_\nu^* ds_+ ds_- . \quad (30)$$

Two approaches were used to extract the statistical uncertainties of Q2B parameters. The first approach uses a linear approximation, whereby errors are evaluated assuming that the likelihood function is a multivariate Gaussian, which is defined by the fit result and covariance matrix. In the second approach we perform a likelihood scan, fixing the scanned Q2B parameter at several consecutive values and repeating the fit to the data. The error on the Q2B parameter is obtained from the shape of the likelihood function near the minimum. Since the Q2B parameters are not directly used in the fit, we fix instead certain parameters that allow the resulting likelihood curve to be trivially interpreted in terms of the Q2B parameter of interest. The likelihood scan approach does not rely on any assumption about the covariance matrix. We use this approach wherever the fit variables that determine a Q2B parameter are found to have non-Gaussian errors.

The Q2B parameters and fit fractions are given together with their statistical and systematic errors in Table 4. It is indicated in the table whether the statistical error has been computed by a likelihood scan or using the linear approximation. Systematic uncertainties are discussed in Section 6. Results of likelihood scans are shown in Figure 5 in terms of $\chi^2 = -2\ln(\mathcal{L})$.

The measured values of $2\beta_{\text{eff}}(f_0(980)K_S^0)$ and $2\beta_{\text{eff}}(\rho^0(770)K_S^0)$ are both consistent with the SM predictions. For the former, the measured value is higher by 2.1 standard deviations compared to that for $b \rightarrow c\bar{c}s$. This is unlike the tendency of other results in $b \rightarrow q\bar{q}s$ transitions. In addition to this, $2\beta_{\text{eff}}(f_0(980)K_S^0) = 0$ is excluded at 4.3σ significance. The phase difference $\Delta\phi(K^{*+}(892)\pi^-, K^{*-}(892)\pi^+)$ is measured here for the first time. A mirror solution at $\sim 35^\circ$ is disfavored at 3.7σ significance. The interval $-102.0^\circ < \Delta\phi(K^{*+}(892)\pi^-, K^{*-}(892)\pi^+) < 135.7^\circ$ is excluded at 95% confidence level (CL).

Note that the values of the Q2B parameters S and C that are obtained from our fit variables must take values within the physical boundary $S^2 + C^2 < 1$, in contrast to the values obtained from Q2B analysis. The value of $S(f_0(980)K_S^0)$ that is obtained is close to the physical boundary and consequently has a highly non-Gaussian uncertainty, as shown in terms of χ^2 in Figure 5. The positive uncertainties on $S(f_0(980)K_S^0)$, including systematics, extracted from this distribution

Table 4: Summary of results for the $Q2B$ parameters. The first quoted error is statistical, the second is systematic and the third is DP signal model uncertainty. Parameters for which the statistical error have been obtained from a likelihood scan are marked by †. Phases are in degrees and relative fractions in %.

Parameter	Value	Parameter	Value
$C(f_0(980)K_S^0)$	$0.35 \pm 0.27 \pm 0.07 \pm 0.04$	$C(\rho^0(770)K_S^0)$	$0.02 \pm 0.27 \pm 0.08 \pm 0.06$
† $2\beta_{\text{eff}}(f_0(980)K_S^0)$	$(89_{-20}^{+22} \pm 5 \pm 8)^\circ$	† $2\beta_{\text{eff}}(\rho^0(770)K_S^0)$	$(37_{-17}^{+19} \pm 5 \pm 6)^\circ$
† $S(f_0(980)K_S^0)$	$-0.94_{-0.02-0.03}^{+0.07+0.05} \pm 0.02$	† $S(\rho^0(770)K_S^0)$	$0.61_{-0.24}^{+0.22} \pm 0.09 \pm 0.08$
$f(f_0(980)K_S^0)$	$14.3_{-1.8}^{+2.8} \pm 1.5 \pm 0.6$	$f(\rho^0(770)K_S^0)$	$9.0 \pm 1.4 \pm 1.1 \pm 1.1$
$A_{CP}(K^{*+}(892)\pi^-)$	$-0.18 \pm 0.10 \pm 0.03 \pm 0.03$	† $\Delta\phi(f_0K_S^0, \rho^0K_S^0)$	$(-59_{-17}^{+16} \pm 6 \pm 6)^\circ$
† $\Delta\phi(K^*(892)\pi)^a$	$(-164 \pm 24 \pm 12 \pm 15)^\circ$		
$f(K^*(892)\pi)$	$11.7 \pm 1.3 \pm 1.3 \pm 0.6$		
$f(K^*(1430)\pi)$	$38.9 \pm 2.5 \pm 0.7 \pm 1.3$	$f(NR)$	$25.6 \pm 2.5 \pm 1.9 \pm 0.5$
$f(f_0(1300)K_S^0)$	$6.3 \pm 1.3 \pm 0.6 \pm 0.3$	$f(f_2(1270)K_S^0)$	$2.1 \pm 0.8 \pm 0.0 \pm 0.2$
$f(\chi_{c0}(1P)K_S^0)$	$1.2 \pm 0.5 \pm 0.0 \pm 0.1$		

^a Abbreviation for $\Delta\phi(K^{*+}(892)\pi^-, K^{*-}(892)\pi^+)$.

are 0.09 at the 32% CL and 0.31 at the 5% CL. The systematic error on S is derived from the corresponding errors on $2\beta_{\text{eff}}$ and C .

To validate the presence of the $f_X(1300)K_S^0$, $f_2(1270)K_S^0$ and $\chi_{c0}(1P)K_S^0$ resonant modes in the signal, we performed fits with three reduced signal models, in which we removed these modes one by one. The differences between these fits and the nominal one in terms of χ^2 for the models missing $f_X(1300)K_S^0$, $f_2(1270)K_S^0$ and $\chi_{c0}(1P)K_S^0$ are 74, 37 and 35, respectively.

As a validation of our treatment of the time-dependence we allow τ_{B^0} and Δm_d to vary in the fit. We find $\tau_{B^0} = (1.579 \pm 0.061)$ ps and $\Delta m_d = (0.497 \pm 0.035)$ ps⁻¹ while the remaining free parameters are consistent with the nominal fit. In addition, we performed a fit floating the S parameters for $B^0 \rightarrow J/\psi K_S^0$ and $B^0 \rightarrow \psi(2S)K_S^0$ events. We measure $S = \sin(2\beta) = 0.690 \pm 0.077$ and 0.73 ± 0.27 for $J/\psi K_S^0$ and $\psi(2S)K_S^0$ respectively. These numbers are in agreement with the current world average for $\sin(2\beta)$. To validate the SCF modeling, we leave the average SCF fractions per tagging category free to vary in the fit and find results that are consistent with the MC estimation.

6 SYSTEMATIC STUDIES

The contributions to the systematic error on the signal parameters are summarized in Table 5.

To estimate the contribution to $B^0 \rightarrow K_S^0 \pi^+ \pi^-$ decay via other resonances, we have first fitted the data including these other decays in the fit model. We considered possible resonances, including $\omega(782)$, $\rho^0(1450)$, $\rho^0(1700)$, $f_0(1710)$, $f_2(1810)$, $K^{*\pm}(1680)$, $K_2^{*\pm}(1430)$, $\chi_{c2}(1P)$ and a low mass S wave σ . A RBW lineshape has been used to parameterize these additional resonances, with masses and widths from [31]. As a second step we have simulated high statistic samples of events, using a model based on the previous fits, including the additional resonances. Finally, we fitted these simulated samples using the nominal signal model. The systematic effect (contained in the ‘‘DP model’’ field in Table 5) is estimated by observing the difference between the generated values and the fitted values corresponding to the generated samples. This systematic effect is quoted separately.

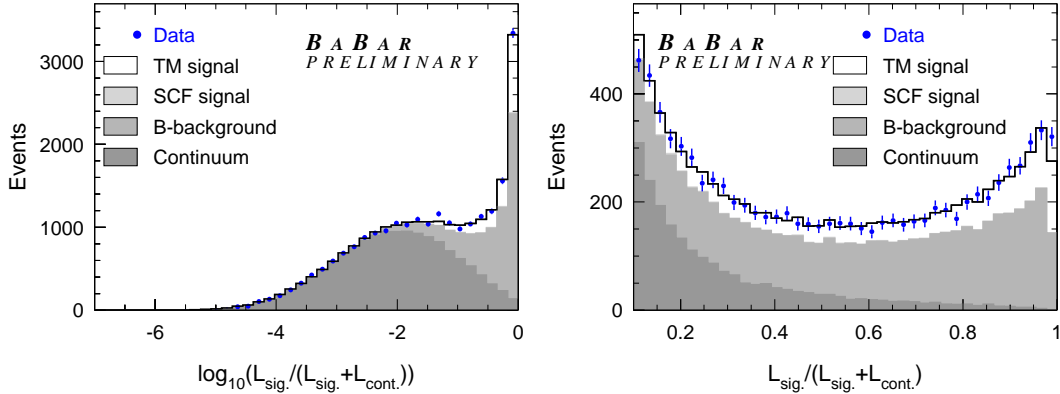


Figure 1: *Distributions of the likelihood ratio (signal/background) for all events entering the fit (left) and in the signal-like region (right). The dots with error bars give the on-resonance data. The solid histogram shows the projection of the fit result. The dark, medium and light shaded areas represent respectively the contribution from continuum events, the sum of continuum events and the B background expectation, and the sum of these and the misreconstructed signal events. The last contribution is hardly visible due to its small fraction. In both distributions the $D^- \pi^+$ and $J/\psi K_S^0$ bands are removed from the DP.*

We vary the mass, width and other parameters (if any) of all components in the fit within their errors, as quoted in Table 1, and assign the observed differences in the measured amplitudes as systematic uncertainties (“lineshape parameters” in Table 5).

To validate the fitting tool, we perform fits on large MC samples with the measured proportions of signal, continuum and B background events. No significant biases are observed in these fits. The statistical uncertainties on the fit parameters are taken as systematic uncertainties (“Fit bias” in Table 5).

Another major source of systematic uncertainty is the B background model. The expected event yields from the background modes are varied according to the uncertainties in the measured or estimated branching fractions. Since B background modes may exhibit CP violation, the corresponding parameters are varied within their uncertainties, or if unknown, within the physical range. As is done for the signal PDFs, we vary the Δt resolution parameters and the flavor-tagging parameters within their uncertainties and assign the differences observed in the data fit with respect to the nominal fit as systematic errors. The systematic uncertainties from these sources are listed as “ B Background” in Table 5.

Other systematic effects are much less important for the measurements of the amplitudes and are combined in the “Other” field in Table 5. Details are given below.

The parameters of continuum PDFs are determined by the fit. No additional systematic uncertainties are assigned to them. An exception to this is the DP PDF: to estimate the systematic uncertainty from the m_{ES} sideband extrapolation, we select large samples of off-resonance data by loosening the requirements on ΔE and the NN output. We compare the distributions of m' and θ' between the m_{ES} sideband and the signal region. No significant differences are found. We assign as systematic error the effect seen when weighting the continuum DP PDF by the ratio of both data sets. This effect is mostly statistical in origin.

The uncertainties associated with Δm_d and τ are estimated by varying these parameters within

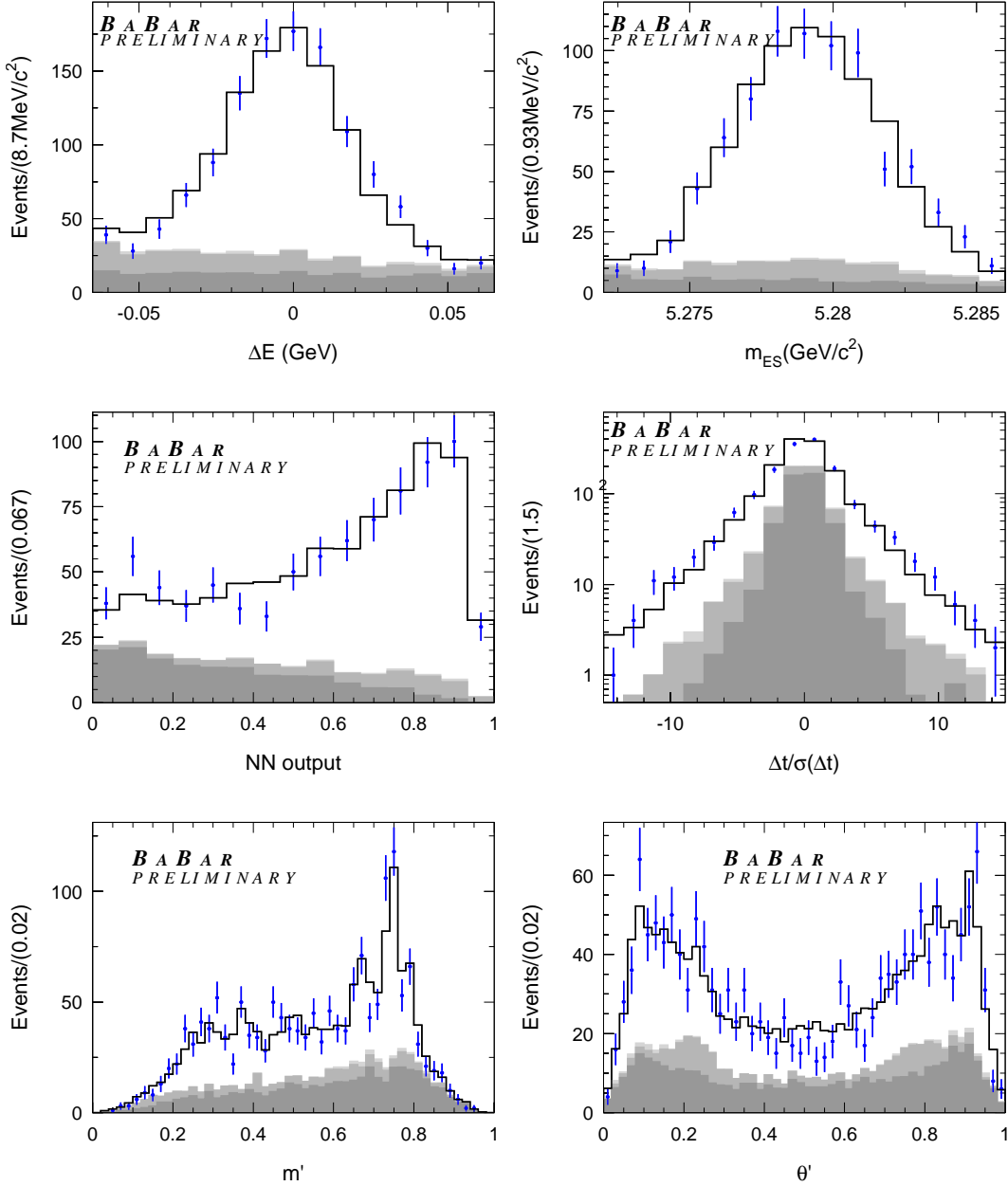


Figure 2: Distributions of (top to bottom, left to right) ΔE , m_{ES} , NN output, $\Delta t/\sigma(\Delta t)$, m' and θ' for samples enhanced in $B^0 \rightarrow K_S^0 \pi^+ \pi^-$ signal. The dots with error bars give the on-resonance data. The solid histogram shows the projection of the fit result. The dark, medium and light shaded areas represent respectively the contribution from continuum events, the sum of continuum events and the B background expectation, and the sum of these and the misreconstructed signal events. The last contribution is hardly visible due to its small fraction. In all these distributions the $D^- \pi^+$ and $J/\psi K_S^0$ bands are removed from the DP.

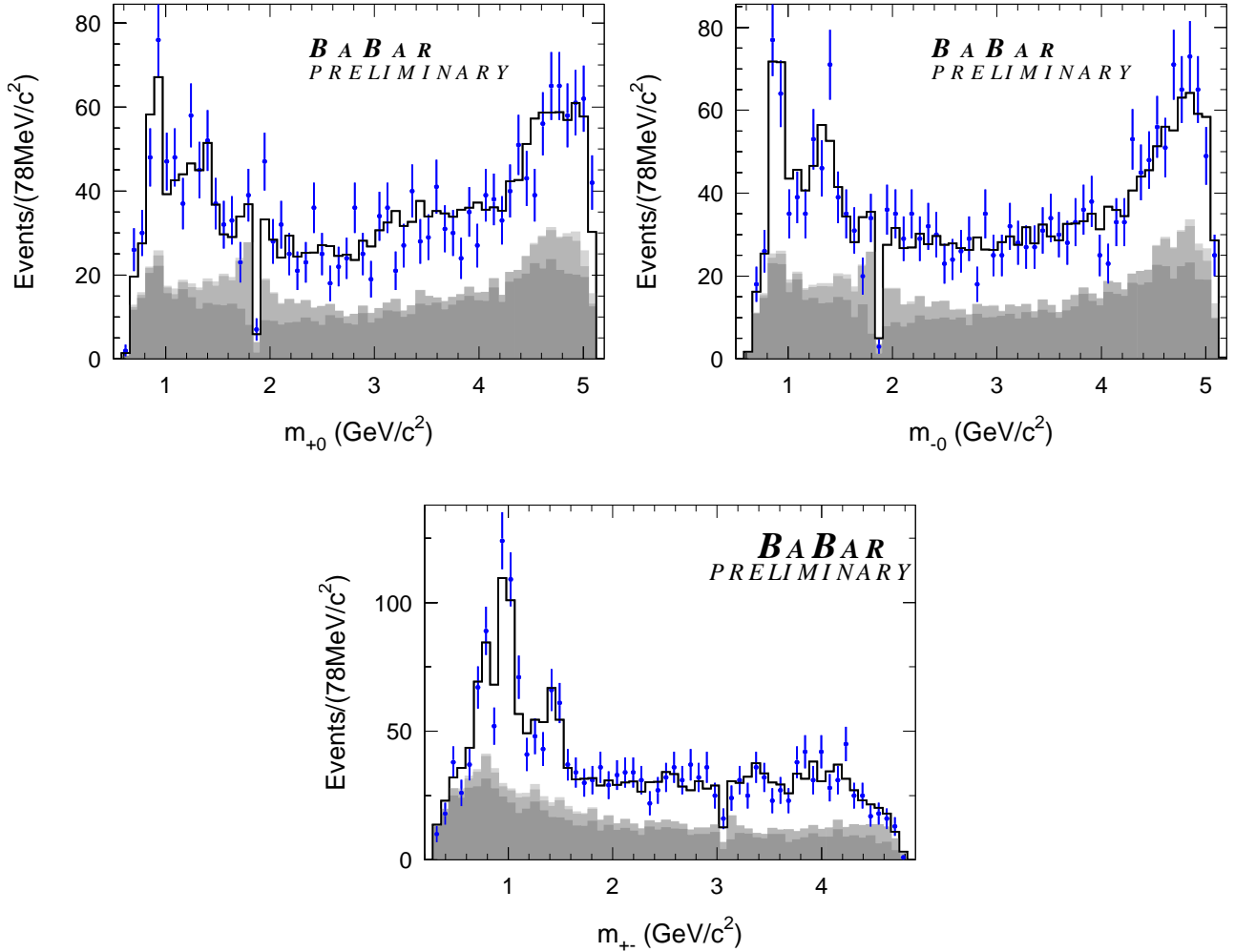


Figure 3: Distributions of $m(K_s^0\pi^+)$ (top left), $m(K_s^0\pi^-)$ (top right), and $m(\pi^+\pi^-)$ (bottom) for samples enhanced in $B^0 \rightarrow K_S^0\pi^+\pi^-$ signal. The solid histogram shows the projection of the fit result. The dark, medium and light shaded areas represent respectively the contribution from continuum events, the sum of continuum events and the B background expectation, and the sum of these and the misreconstructed signal events. The last contribution is hardly visible due to its small fraction. In all these distributions the $D^-\pi^+$ and $J/\psi K_S^0$ bands are removed from the DP.

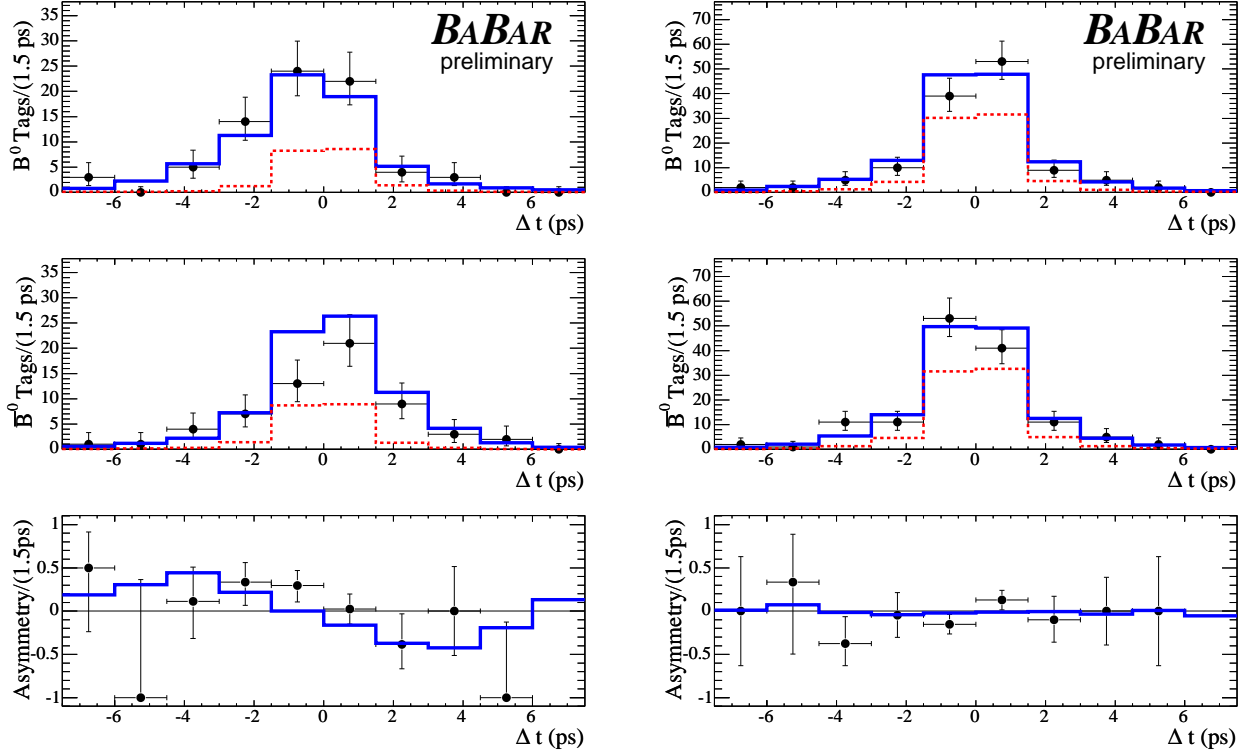


Figure 4: Distributions of Δt when the B_{tag}^0 is a B^0 (top), \bar{B}^0 (middle) and the derived Δt asymmetry (bottom). Plots on the left (right) hand side, correspond to events in the $f_0(980)K_S^0$ ($\rho^0(770)K_S^0$) region. The solid line is the total PDF, the dashed line is the continuum only PDF and points with error bars represent data. These distributions correspond to samples enhanced in $B^0 \rightarrow K_S^0 \pi^+ \pi^-$ signal, where the $D^- \pi^+$ and $J/\psi K_S^0$ bands are removed from the DP.

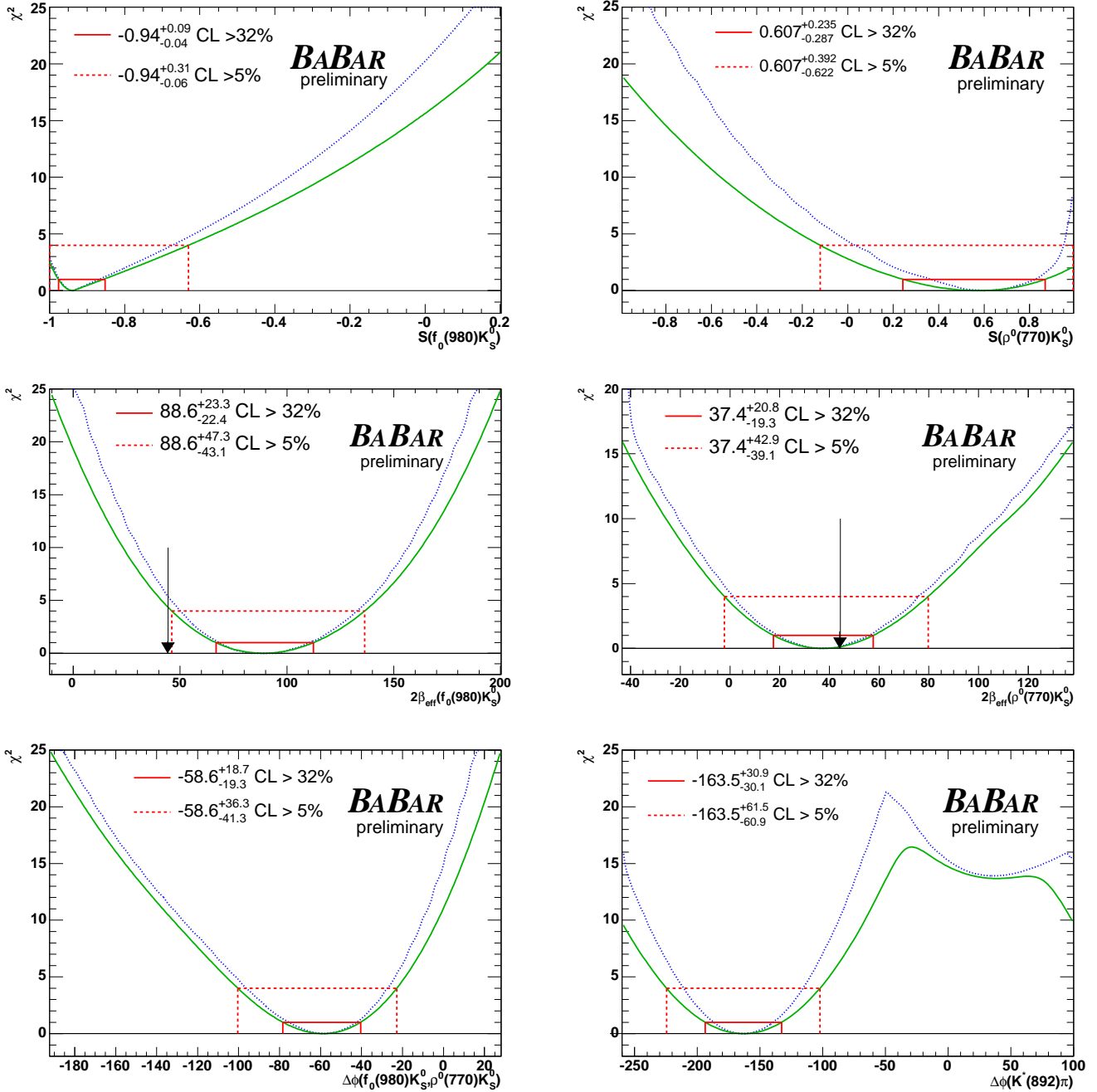


Figure 5: Results of likelihood scans in terms of $\chi^2 = -2\ln(\mathcal{L})$ for the Q2B parameters (left to right, top to bottom): $S(f_0(980)K_S^0)$, $S(\rho^0(770)K_S^0)$, $2\beta_{\text{eff}}(f_0(980)K_S^0)$, $2\beta_{\text{eff}}(\rho^0(770)K_S^0)$, $\Delta\phi(f_0(980)K_S^0, \rho(770)K_S^0)$ and $\Delta\phi(K^{*+}(892)\pi^-, K^{*-}(892)\pi^+)$. The solid (dotted) curves corresponds to the total (statistical) error. Indicated by solid (dashed) rectangles are the parameter values corresponding to 1σ (2σ). The arrows mark the measured values in $b \rightarrow c\bar{c}s$ transitions [3].

the uncertainties on the world average [31].

The signal PDFs for the Δt resolution and tagging fractions are determined from fits to a control sample of fully reconstructed B decays to exclusive final states with charm, and the uncertainties are obtained by varying the parameters within the statistical uncertainties.

The average fraction of misreconstructed signal events predicted by the MC simulation has been verified with fully reconstructed $B \rightarrow D\rho$ events [38]. No significant differences between data and the simulation were found. We vary \bar{f}_{SCF} for all tagging categories relatively by 25% to estimate the systematic uncertainty. Tagging efficiencies, dilutions and biases for signal events are varied within their experimental uncertainties.

7 SUMMARY

We have presented preliminary results from a time-dependent Dalitz plot analysis of $B^0 \rightarrow K_S^0 \pi^+ \pi^-$ decays obtained from a data sample of 383 million $\Upsilon(4S) \rightarrow B\bar{B}$ decays. We measure 15 pairs of relative phases and magnitudes for the different resonances, taking advantage of the interference between them in the Dalitz plot. From the measured decay amplitudes, we derive the Q2B parameters of the resonant decay modes. In particular, the mixing-induced CP asymmetry S is extracted from the measured amplitudes. The measured values of $2\beta_{\text{eff}}$ in B^0 decays to $f_0(980)K_S^0$ and $\rho^0(770)K_S^0$ are $(89_{-20}^{+22} \pm 5 \pm 8)^\circ$ and $(37_{-17}^{+19} \pm 5 \pm 6)^\circ$, respectively. These results are both consistent with the SM predictions, but in the case of $B^0 \rightarrow f_0(980)K_S^0$ the measured value is higher by 2.1 standard deviations compared to that for $b \rightarrow c\bar{c}s$. This is unlike the tendency of other results in $b \rightarrow q\bar{q}s$ transitions. Also, $2\beta_{\text{eff}}(f_0(980)K_S^0) = 0$ is excluded at 4.3σ significance.

In decays to $K^*(892)\pi$ we find $A_{CP} = -0.18 \pm 0.10 \pm 0.03 \pm 0.03$. The phase difference $\Delta\phi$ between the amplitudes of $B^0 \rightarrow K^{*+}(892)\pi^-$ and $\bar{B}^0 \rightarrow K^{*-}(892)\pi^+$ is measured for the first time. We find $\Delta\phi = (-164 \pm 24 \pm 12 \pm 15)^\circ$, and mirror solutions are disfavored at $\sim 3.7\sigma$ significance. The interval $-102^\circ < \Delta\phi < 136^\circ$ is excluded at 95% confidence level. Our results may be used to extract the CKM angle γ following the methods proposed in Refs. [18, 19, 20, 21].

8 Acknowledgments

We are grateful for the extraordinary contributions of our PEP-II colleagues in achieving the excellent luminosity and machine conditions that have made this work possible. The success of this project also relies critically on the expertise and dedication of the computing organizations that support *BABAR*. The collaborating institutions wish to thank SLAC for its support and the kind hospitality extended to them. This work is supported by the US Department of Energy and National Science Foundation, the Natural Sciences and Engineering Research Council (Canada), the Commissariat à l’Energie Atomique and Institut National de Physique Nucléaire et de Physique des Particules (France), the Bundesministerium für Bildung und Forschung and Deutsche Forschungsgemeinschaft (Germany), the Istituto Nazionale di Fisica Nucleare (Italy), the Foundation for Fundamental Research on Matter (The Netherlands), the Research Council of Norway, the Ministry of Science and Technology of the Russian Federation, Ministerio de Educación y Ciencia (Spain), and the Science and Technology Facilities Council (United Kingdom). Individuals have received support from the Marie-Curie IEF program (European Union) and the A. P. Sloan Foundation.

	$C(f_0(980)K_S^0)$	$2\beta_{\text{eff}}(f_0(980)K_S^0)$	$f(f_0(980)K_S^0)[\%]$
DP model	0.04	7.8	0.6
Lineshape parameters	0.06	3.9	1.0
B background	0.03	2.7	0.4
Fit bias	0.01	1.1	1.0
Other	0.03	1.4	0.1
Sum w/o DP model	0.07	5.1	1.5
Total sum	0.08	9.3	1.6

	$C(\rho^0(770)K_S^0)$	$2\beta_{\text{eff}}(\rho^0(770)K_S^0)$	$f(\rho^0(770)K_S^0)[\%]$
DP model	0.06	5.9	1.1
Lineshape parameters	0.04	3.6	0.3
B background	0.06	3.8	0.1
Fit bias	0.02	0.4	1.0
Other	0.02	1.0	0.1
Sum w/o DP model	0.08	5.3	1.1
Total sum	0.10	7.9	1.5

	$A_{CP}(K^{*+}\pi^-)$	$f(K^{*+}\pi^-)[\%]$	$\Delta\phi(K^{*+}\pi^-, K^{*-}\pi^+)$	$\Delta\phi(f_0K_S^0, \rho^0K_S^0)$
DP model	0.03	0.6	15.0	6.0
Lineshape parameters	0.01	0.2	4.3	4.2
B background	0.03	0.3	4.5	4.3
Fit bias	0.01	1.2	9.7	0.3
Other	0.00	0.1	2.6	1.7
Sum w/o DP model	0.03	1.3	11.8	6.3
Total sum	0.05	1.4	19.1	8.7

Table 5: Summary of systematic uncertainties. Errors on $2\beta_{\text{eff}}$ and $\Delta\phi$ are given in degrees and relative fractions in %. $K^{*\pm}$ refer to $K^{*\pm}(892)$.

References

- [1] Cabibbo, N., *Phys. Rev. Lett.*, **10**:531, 1963.
- [2] Kobayashi, M. and Maskawa, T., *Prog. Theor. Phys.*, **49**:652, 1973.
- [3] Barberio, E. *et al.*, Heavy Flavor Averaging Group (HFAG), 2006, hep-ex/0704.3575.
- [4] Grossman, Y., Ligeti, Z., Nir, Y., and Quinn, H., *Phys. Rev.*, **D68**:015004, 2003.
- [5] Gronau, M., Grossman, Y., and Rosner, J. L., *Phys. Lett.*, **B579**:331, 2004.
- [6] Gronau, M., Rosner, J. L., and Zupan, J., *Phys. Lett.*, **B596**:107, 2004.
- [7] Cheng, H.-Y., Chua, C.-K., and Soni, A., *Phys. Rev.*, **D72**:014006, 2005.
- [8] Gronau, M. and Rosner, J. L., *Phys. Rev.*, **D71**:074019, 2005.
- [9] Beneke, M., *Phys. Lett.*, **B620**:143, 2005.
- [10] Engelhard, G., Nir, Y., and Raz, G., *Phys. Rev.*, **D72**:075013, 2005.
- [11] Cheng, H.-Y., Chua, C.-K., and Soni, A., *Phys. Rev.*, **D72**:094003, 2005.
- [12] Williamson, A. R. and Zupan, J., *Phys. Rev.*, **D74**:014003, 2006.
- [13] Gershon, T. and Hazumi, M., *Phys. Lett.*, **B596**:163, 2004.
- [14] Belle Collaboration, Garmash, A. *et al.*, *Phys. Rev.*, **D69**:012001, 2004.
- [15] BABAR Collaboration, Aubert, B. *et al.*, hep-ex/0706.3885, 2007, submitted to *Phys. Rev. Lett.*
- [16] Wolfenstein, L., *Phys. Rev. Lett.*, **51**:1945, 1983.
- [17] Buras, A. J., Lautenbacher, M. E., and Ostermaier, G., *Phys. Rev.*, **D50**:3433, 1994.
- [18] Deshpande, N. G., Sinha, N., and Sinha, R., *Phys. Rev. Lett.*, **90**:061802, 2003.
- [19] Ciuchini, M., Pierini, M., and Silvestrini, L., *Phys. Rev.*, **D74**:051301, 2006.
- [20] Gronau, M., Pirjol, D., Soni, A., and Zupan, J., *Phys. Rev.*, **D75**:014002, 2007.
- [21] Lipkin, H. J., Nir, Y., Quinn, H. R., and Snyder, A., *Phys. Rev.*, **D44**:1454, 1991.
- [22] Belle Collaboration, Garmash, A. *et al.*, *Phys. Rev.*, **D75**:012006, 2007.
- [23] BABAR Collaboration, Aubert, B. *et al.*, *Phys. Rev.*, **D73**:031101, 2006.
- [24] Belle Collaboration, Chang, P. *et al.*, *Phys. Lett.*, **B599**:148, 2004.
- [25] BABAR Collaboration, Aubert, B. *et al.*, hep-ex/0408073, 2004.
- [26] BABAR Collaboration, Aubert, B. *et al.*, *Phys. Rev.*, **D72**:072003, 2005, Erratum-
ibid.D74:099903,2006.
- [27] Belle Collaboration, Garmash, A. *et al.*, *Phys. Rev. Lett.*, **96**:251803, 2006.

- [28] BABAR Collaboration, Aubert, B. *et al.*, *Phys. Rev. Lett.*, **93**:131801, 2004.
- [29] Belle Collaboration, Abe, K. *et al.*, hep-ex/0507045, 2005.
- [30] Blatt, J. and Weisskopf, V. E., *Theoretical Nuclear Physics*, J. Wiley (New York), 1952.
- [31] Particle Data Group Collaboration, Yao, W. M. *et al.*, *J. Phys.*, **G33**:1, 2006, and 2007 partial update for the 2008 edition.
- [32] Flatte, S. M., *Phys. Lett.*, **B63**:224, 1976.
- [33] Gounaris, G. J. and Sakurai, J. J., *Phys. Rev. Lett.*, **21**:244, 1968.
- [34] LASS Collaboration, Aston, D. *et al.*, *Nucl. Phys.*, **B296**:493, 1988.
- [35] Bugg, D. V., *Phys. Lett.*, **B572**:1, 2003.
- [36] BES Collaboration, Ablikim, M. *et al.*, *Phys. Lett.*, **B607**:243, 2005.
- [37] Dunwoodie, W. M., private communication.
- [38] BABAR Collaboration, Aubert, B. *et al.*, *Phys. Rev.*, **D76**:012004, 2007.
- [39] BABAR Collaboration, Aubert, B. *et al.*, *Nucl. Instrum. Meth.*, **A479**:1, 2002.
- [40] Gay, P., Michel, B., Proriol, J., and Deschamps, O., prepared for 4th International Workshop on Software Engineering and Artificial Intelligence for High-energy and Nuclear Physics (AIHENP 95), Pisa, Italy, 3-8 April 1995.
- [41] BABAR Collaboration, Aubert, B. *et al.*, *Phys. Rev. Lett.*, **94**:161803, 2005.
- [42] Gardner, S. and Tandean, J., *Phys. Rev.*, **D69**:034011, 2004.
- [43] Skwarnicki, T., Ph.D. thesis, DESY-F31-86-02, 1986, appendix E.
- [44] Oreglia, M., Ph.D. thesis, SLAC-0236, 1980, appendix D.
- [45] Gaiser, J., Ph.D. thesis, SLAC-0255, 1982, appendix F.
- [46] ARGUS Collaboration, Albrecht, H. *et al.*, *Z. Phys.*, **C48**:543, 1990.